Lensless Imaging with Compressive Ultrafast Sensing

Guy Satat, Matthew Tancik and Ramesh Raskar

arXiv:1610.05834v1 [cs.CV] 19 Oct 2016

***Abstract*—Conventional imaging uses a set of lenses to form an image on the sensor plane. This pure hardware-based approach doesn't use any signal processing, nor the extra information in the time of arrival of photons to the sensor. Recently, modern compressive sensing techniques have been applied for lensless imaging. However, this computational approach tends to depend as much as possible on signal processing (for example, single pixel camera) and results in a long acquisition time. Here we propose using compressive ultrafast sensing for lensless imaging. We use extremely fast sensors (picosecond time resolution) to time tag photons as they arrive to an omnidirectional pixel. Thus, each measurement produces a time series where time is a function of the photon source location in the scene. This allows lensless imaging with significantly fewer measurements compared to regular single pixel imaging ($33\times$ less measurements in our experiments). To achieve this goal, we developed a framework for using ultrafast pixels with compressive sensing, including an algorithm for ideal sensor placement, and an algorithm for optimized active illumination patterns. We show that efficient lensless imaging is possible with ultrafast imaging and compressive sensing. This paves the way for novel imaging architectures, and remote sensing in extreme situations where imaging with a lens is not possible.**

I. Introduction

TRADITIONAL imaging is based on lenses that map the scene plane to the sensor plane. This physics-based approach requires no computation or signal processing, thus the imaging quality depends on parameters such as lens quality and numerical aperture, density of the sensor array and pixel size. Recently it has been challenged by modern signal processing techniques. Fundamentally the goal is to transfer most of the burden of imaging from high quality hardware to computation. This is known as computational imaging, in which the measurement encodes the target features; these are later computationally decoded to produce the desired image. Furthermore, the end goal is to completely eliminate the need for high quality lenses, which are heavy, bulky, and expensive.

One of the key workhorses in computational imaging is compressive sensing (CS) [1], [2]. For example, CS enabled the single pixel camera [3], which demonstrated imaging with a single pixel that captured scene information encoded with a spatial light modulator (SLM). The pixel took multiple consecutive measurements, each one with a different SLM pattern. The measurements were then inverted to recover the scene using compressive deconvolution.

Broadly, the traditional imaging and single pixel camera demonstrate two extremes: on the one hand pure hardware approach, and on the other hand an effort to minimize the requirement for high quality hardware using modern signal processing. There are many trade-offs between the two approaches. One notable difference is the overall acquisition time: the physics-based approach requires one measurement (i.e. all the sensing is done in parallel), which enables a single shot acquisition, while the single pixel camera and its variants require hundreds of consecutive measurements, which translates into a substantially longer acquisition time.

In this paper we present a method that combines the best of the two, specifically time-resolved sensing (an advanced physical measurement hardware) combined with compressive sensing (like the single pixel camera). This results in lensless imaging with $33\times$ less measurements compared to a regular single pixel camera.

Time-resolved imaging is achieved by using pulsed active illumination combined with a sensor with time resolution in the order of picosecond (ps). PS time resolution allows distinguishing between photons that arrive from different parts of the target with mm resolution. The sensor provides more information per measurement (compared to regular pixel), and so less measurements are needed. Moreover, the time-resolved sensor is characterized by a measurement operator that enables us to choose ideal active illumination patterns to reduce the number of measurements even further.

A. Contributions

The contributions presented in this paper can be summarized as follows:

1) Computational imaging framework for lensless imaging with compressive time-resolved measurement,
2) Analysis of a time-resolved sensor as an imaging pixel,
3) Algorithm for ideal sensor placement within a defined region,
4) Algorithm for ideal illumination patterns.

B. Related Works

1) Compressive Sensing for Imaging: Compressive sensing has been driving many novel imaging modalities. Examples include: ultra-spectral imaging [4], subwavelength imaging [5], wavefront sensing [6], holography [7], imaging through scattering media [8] and terahertz imaging [9].

2) Single Pixel Imaging: One of the most notable applications of compressive sensing in imaging is the single pixel camera [3]. This was later extended to general imaging with masks [10]. We refer the interested reader to an introduction on imaging with compressive sampling in [11].

G. Satat, M. Tancik and R. Raskar are with the Media Lab, Massachusetts Institute of Technology, Cambridge, MA, 02139 USA. e-mail: guysatat@mit.edu.

Other communities have also discussed the use of indirect measurements for imaging. In the physics community the concept of using a single pixel (bucket) detector to perform imaging is known as ghost imaging and was initially thought of as a quantum phenomenon [12]. It was later realized that computational techniques can achieve similar results [13]. Ghost imaging was also incorporated with compressive sensing [14], [15]. In the computational imaging community the concept of indirect imaging is known as dual photography [16].

Single pixel imaging extends to multiple sensor. For example, multiple sensors were used for 3D reconstruction of a scene by using stereo reconstruction [17]. Multiple sensors were also incorporated with optical filters to create color images [18].

In this work we suggest using a time-resolved sensor as opposed to a regular bucket detector for lensless imaging.

3) Time-Resolved Sensing for Imaging: Time-resolved sensing has been mostly used to recover scene geometry. This is known as LIDAR, e.g. [19], [20]. Time-resolved sensing has also been suggested to recover scene reflectance [21], [22] for lensless imaging, but didn't discuss the use of structured illumination and compressive sensing. Other examples of time-resolved sensing include non-line of sight imaging, for example imaging behind a corner [23] and through scattering layers [24].

In this paper we use compressive deconvolution with time-resolved sensing for lensless imaging to recover target reflectance.

C. Limitations

The main limitations of using our suggested approach are:

- We assume a linear imaging model (linear modeling in imaging is common, for example [3], [10]).
- Our current implementation assumes a planar scene. We note that our approach can naturally extend to piecewise planar scenes and leave this extension to a future study.
- Time-resolved sensing requires an active pulsed illumination source and a time-resolved sensor. These can be expensive and complicated to set up. However, as we demonstrate here, they provide a different set of trade-offs for lensless imaging, primarily reduced acquisition time.

II. Compressive Ultrafast Sensing

Our goal is to develop a framework for compressive imaging with time-resolved sensing. Fig. 1 shows the system overview. A time pulsed source is modulated to produce wavefront $\mathbf{G}$, which illuminates the scene $\mathbf{f}$. Light from the scene is measured by an omnidirectional ultrafast sensor (or sensors) positioned on the sensor plane. $\mathbf{H}$ represents the space to time mapping that is enforced by special relativity. We assume a linear measurement process, i.e. the measurement $\widetilde{\mathbf{m}}$ is a linear combination of the target $\mathbf{f}$ ($\mathbf{f}$ is the vectorized target reflectance image), such that: $\widetilde{\mathbf{m}} = \mathbf{Q}\mathbf{f}$ where $\mathbf{Q}$ is the measurement operator. Obviously this is an underdetermined system, and our goal is to invert it. To that end, we analyze and physically modify $\mathbf{Q}$ to make the inversion robust. In the remainder of this paper we analyze and optimize these fundamental components of $\mathbf{Q}$:

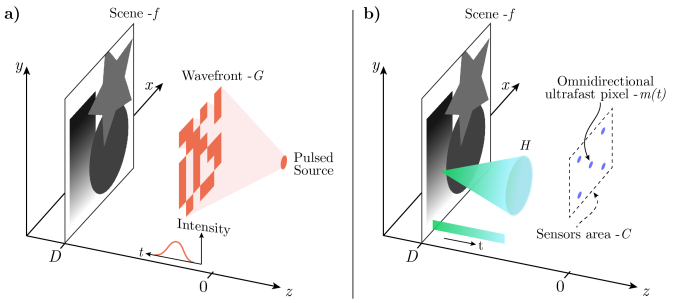

Fig. 1. Lensless imaging with compressive ultrafast sensing. a) Illumination, a time pulsed source is wavefront modulated ($\mathbf{G}$) and illuminates a target with reflectance $\mathbf{f}$. b) Measurement, omnidirectional ultrafast sensor (or sensors) measure the time dependent response of the scene $\mathbf{m}(t)$. $\mathbf{H}$ is a causality operator that maps scene pixels to the time-resolved measurement.

- Physics-based time-resolved light transport operator $\mathbf{H}$. $\mathbf{H}$ is a mapping from the spatial coordinates of the scene domain to the time-resolved measurement ($\mathbf{H} : r \rightarrow t$). Section III derives a physical model of $\mathbf{H}$ and discusses its structure and properties. $\mathbf{H}$ can be modified by changing the sensor time resolution and position in the sensor plane.
- Combination of multiple sensors. We can place multiple sensors in the sensor plane, such that each sensor will correspond to a different time-resolved light transport $\mathbf{H}_i$. Section IV presents an algorithm for optimized sensor placement in the sensor plane.
- Illumination (probing) operator $\mathbf{G}$. This operator is similar to the sensing matrix in the single pixel camera case which was realized then with an SLM. In our analysis we assume the modulation is performed on the illumination side (but note that modulating the illumination is equivalent to modulating the incoming wavefront to the sensor). The structured illumination allows modulating the illumination amplitude on different pixels in the target. We consider multiple illumination patterns such that $\mathbf{G}_j$ corresponds to the j-th illumination pattern. Section V presents an algorithm for optimized illumination patterns for compressive ultrafast imaging.

The time-resolved measurement of the i-th sensor, for a scene illuminated by the j-th illumination pattern, is defined by: $\mathbf{m}_{i,j} = \mathbf{H}_i\mathbf{G}_j\mathbf{f}$. We note that $\mathbf{m}_{i,j}$ is a vector with N time samples (N increases with better time resolution, denoted by T). The scene size is $L \times L$ pixels, such that $\mathbf{H}_i$ is an $N \times L^2$ matrix. Stacking all measurement vectors together results in the total measurement vector $\widetilde{\mathbf{m}}$, such that the total measurement process is:

$$\widetilde{\mathbf{m}} = \begin{bmatrix} \vdots \\ \mathbf{m}_{i,j} \\ \vdots \end{bmatrix} = \begin{bmatrix} \vdots \\ \mathbf{H}_i\mathbf{G}_j \\ \vdots \end{bmatrix} \mathbf{f} = \mathbf{Q}\mathbf{f} \qquad (1)$$

We consider K sensors ($i = 1..K$) and M illumination patterns ($j = 1..M$) so $\mathbf{Q}$ is an $NKM \times L^2$ matrix.

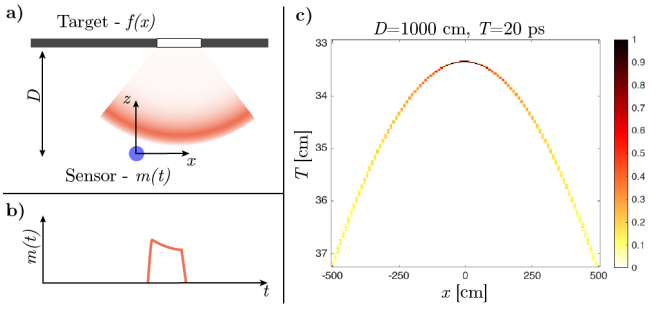

Fig. 2. Analysis of a one dimensional world. a) Geometry, the target is a black line with a white patch, at a distance D from the time-resolved sensor. b) The time-resolved measurement produced by the sensor. The rise time corresponds to the patch distance, and the time duration to the patch width. c) The measurement matrix H, generated from Eq. 8. Here the distance to the target is $D = 10m$ and the sensor has a time resolution of $T = 20ps$.

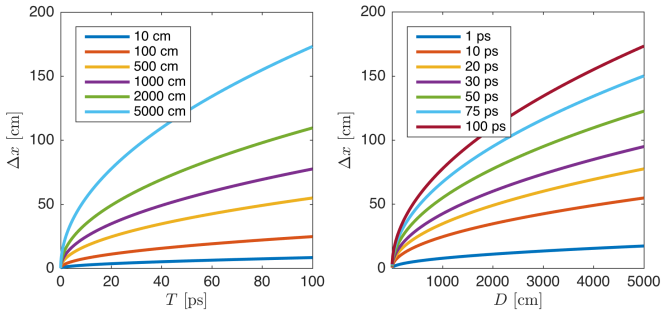

Fig. 3. Recoverable resolution with time-resolved sensing. a) Plots for various scene distances D as a function of sensor time resolution T. b) Plots for various sensor time resolutions as a function of target distance D.

In the case where time resolution is very poor, $\mathbf{H}$ is just a single row ($N = 1$), and the process is reduced to the regular single pixel camera case. The interesting measurement occurs when $NKM \ll L^2$. Then in order to invert Eq. 1 we use a compressive sensing approach. The inversion is robust if the mutual coherence of $\mathbf{Q}$ is low enough [25]. The mutual coherence is a measure for the worst similarity of the matrix columns, and is defined by:

$$\mu\{\mathbf{Q}\} = \max_{1\leq a,b\leq L^2, a\neq b} \frac{\left|\mathbf{Q}_a{}^T \mathbf{Q}_b\right|}{\|\mathbf{Q}_a\| \, \|\mathbf{Q}_b\|} \tag{2}$$

As suggested in [25], a different way to use the concept of mutual coherence is the Gramm matrix: $\mathbf{O} = \tilde{\mathbf{Q}}^T\tilde{\mathbf{Q}}$, where $\tilde{\mathbf{Q}}$ is $\mathbf{Q}$ with columns normalized to unity. Based on Eq. 2 and the definition of the Gramm matrix, the mutual coherence is the largest off diagonal element in $\mathbf{O}$. Thus, it is possible to relax the demand of calculating the mutual coherence, and instead measure how close the Gramm matrix is to the identity. This directly targets the restricted isometry property (RIP) [26], which provides guarantees for using compressive sensing. This can be written as:

$$\bar{\mu} = \frac{1}{L^2}\left\|\mathbf{I}_{L^2} - \tilde{\mathbf{Q}}^T\tilde{\mathbf{Q}}\right\|_F^2 \tag{3}$$

where $\mathbf{I}_{L^2}$ is the identity matrix of size L^2. In the remainder of the paper we optimize different parts of $\mathbf{Q}$ using this measure of coherence as a cost objective.

III. Time-Resolved Light Transport

Currently, there are many time-resolved sensors that provide a wide range of implementation options, as surveyed in Appendix A. We start by developing a generic light transport model for time-resolved imaging. The finite speed of light governs information propagation, and provides geometrical constraints which will be used in the image formation model. These are conveniently described in a Minkowski space with the space-time four-vector $\mathbf{v} = (r,t) = (x,y,z,t)$. If we consider a point source at position r' pulsing at time t', and a sensor at position r, then the space-time interval between the source $\mathbf{v}' = (r',t')$ and the sensor $\mathbf{v} = (r,t)$ is defined by:

$$s^2 = (\mathbf{v}-\mathbf{v}')\circ(\mathbf{v}-\mathbf{v}') = \|r-r'\|_2^2 - c^2(t-t')^2 \tag{4}$$

where c is the speed of light. Causality requires lightlike behavior, i.e. $s^2 = 0$, which is known as the light cone (Fig. 1b shows a schematic of the light cone). To enforce the light cone space-time geometry we define:

$$l(r,t) = \begin{cases} 1 & \|r\|_2^2 - c^2t^2 = 0 \\ 0 & else \end{cases} \tag{5}$$

This allows writing the time-resolved measurement to a general time dependent scene $\mathbf{f}(r',t')$ as:

$$m(r,t) = \int_{-\infty}^{t}\int_{V} \frac{1}{c^2t^2} f(r',t')\, l(r-r',t-t')\, dr'dt' \tag{6}$$

where V is the target volume of interest, and the $1/(ct)^2$ term accounts for the $1/\|r\|_2^2$ intensity drop off (where we use $(ct)^2 = \|r-r'\|_2^2$).

Next, we assume a planar scene at $z = D$ and a stationary target. We use the circular symmetry of the light cone so that:

$$m(x,y,t) = \int_0^{2\pi} \frac{1}{c^2t^2} f(x+\rho\cos(\theta'), y+\rho\sin(\theta'))\,\rho d\theta' \tag{7}$$

with $\rho = \sqrt{c^2t^2 - D^2}$.

The sensor's finite time resolution T corresponds to the sampling of $m(x,y,t)$. And finally, a sensor positioned at location $r_i = (x_i, y_i)$ will produce a measurement $\mathbf{m}_i(t) = \mathbf{H}_i\mathbf{f}$, where $\mathbf{H}_i$ is defined by the kernel in Eq. 7.

A. One Dimensional Analysis

It is interesting to analyze $\mathbf{H}$ in a planar world ($y = 0$) with the sensor at the origin (Fig. 2a). In that case Eq. 7 simply becomes:

$$m(t) = \frac{1}{c^2t^2}\left[f\left(-\sqrt{c^2t^2 - D^2}\right) + f\left(\sqrt{c^2t^2 - D^2}\right)\right] \tag{8}$$

Fig. 2b shows an example of the corresponding H matrix. This toy example demonstrates the key properties of the time-resolved measurement: 1) It is a nonlinear mapping of space to time. 2) The mapping is not unique (two opposite space points are mapped to the same time slot). 3) Spatial points that are close to the sensor are measured in an underdetermined way (adjacent pixels mapped to the same time slot). 4) Spatial points that are far from the sensor are measured in an overdetermined way, but they are of a weaker signal. These properties affect imaging parameters as described next:

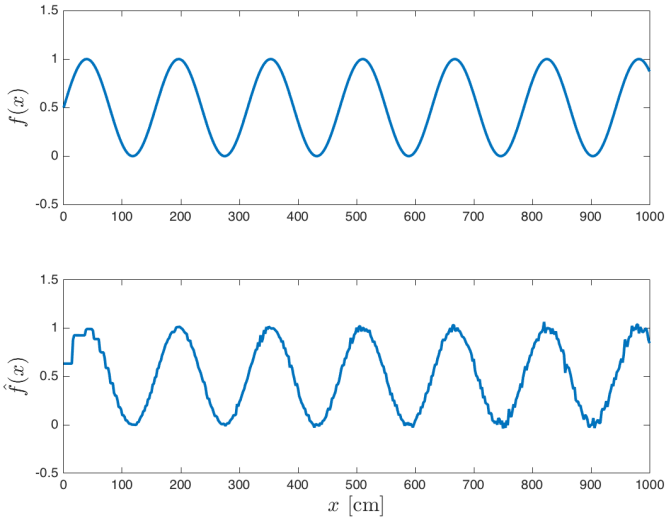

Fig. 4. Effects of averaging and noise on time-resolved measurement. $f(x)$ is a sinusoid on the positive half plane, at a distance $D = 10m$ from a sensor with time resolution $T = 20ps$ and measurement noise of $SNR = 35dB$. $\hat{f}(x)$ is the inversion of the measurement using the Moore-Penrose pseudoinverse, which demonstrates the underdetermined measurement close to the sensor, and sensitivity to noise further away from the sensor.

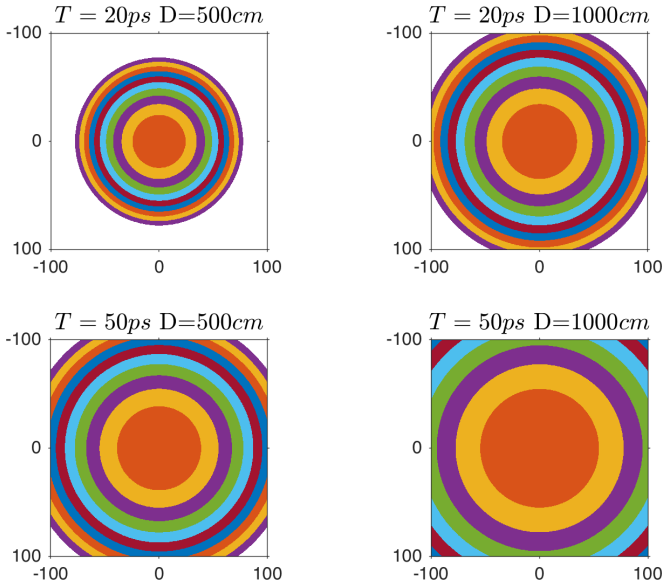

Fig. 5. Measurement of a planar scene for various sensor time resolutions (T) and target distances (D). The color represents time samples indexes (for the first 10 samples). As the time resolution worsens or the target is further away, the rings become thicker. The images show a subset area of $100 \times 100cm^2$.

1) Resolution limit: The minimum recoverable spatial resolution is defined by the closest point to the sensor: $ct_1 = D$, and the point that corresponds to the next time slot: $c(t_1 + T) = \sqrt{D^2 + \Delta x^2}$, which results in :

$$\Delta x = cT\sqrt{1 + 2\frac{D}{cT}} \tag{9}$$

Fig. 3 shows a few cross sections of Eq. 9 for relevant distances D and time resolution T. Better time resolution is required for further scenes (for the same recoverable resolution).

2) Signal to noise ratio and dynamic range limitation: The closest point to the sensor defines the measurement gain (in order to avoid the saturation intensity I_{sat}), such that $I_{sat} > A\left(D^2\right)^{-1}$, where A accounts for all measurement constants. The furthest measurable point from the sensor (x_{max}) should result in a measurement above the noise floor: $I_n < A\left(D^2 + x_{max}^2\right)^{-1}$.

Since the signal to noise ratio (SNR) is proportional to the gain, closer scenes will have smaller coverage areas. For example, if we assume: $I_{sat} = BI_n$ (for some constant $B > 1$) we get: $x_{max} < \sqrt{B-1}D$.

The combined effect of these phenomena is demonstrated in Fig. 4. In this example, we consider a 'half world' ($x > 0$), where the target reflectance is $f(x) = sin(x)$ with additive white Gaussian noise, which results in $SNR = 35dB$. For this simple demonstration, we use the Moore-Penrose pseudoinverse to invert the measurement, such that $\hat{f} = H^{\dagger}m$. The inversion shows that close to the origin ($x < 50cm$) the reconstruction suffers from an underdetermined measurement, this area is not sensitive to the measurement noise, and looks identical with zero noise. The noise has an obvious effect on the reconstruction further from the origin ($x > 700cm$).

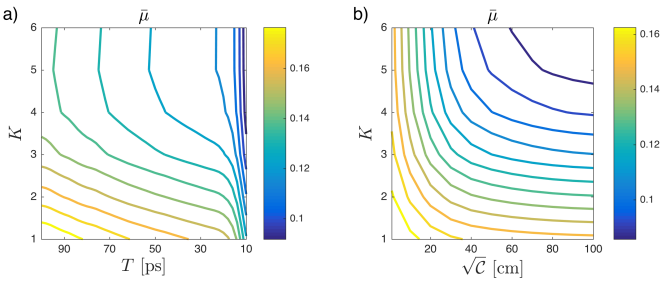

Fig. 6. Effect of number of sensors K, their time resolution T, and array size constraint $\mathcal{C}$ on the mutual coherence $\bar{\mu}$ evaluated with Eq. 3. a) Mutual coherence isobars for a varying number of sensors and their time resolution (for fixed array size $\sqrt{\mathcal{C}} = 10cm$). b) Similar to (a) with varying array size constraint (for fixed time resolution $T = 20ps$).

B. Analysis of a planar scene

All the properties presented in the previous subsection extend to the case of a planar scene. Eq. 7 shows that the measurement process integrates over circles centered around the sensor. Due to the finite time resolution, the circles are mapped to rings with smaller thickness for further points, according to $\rho_n = \sqrt{c^2(nT + t_0)^2 - D^2}$, where n is the time sample number and $t_0 = D/c$ is the time of arrival from the closest point. Fig. 5 shows the ring structure for a few cases of time resolution and target distance.

Lastly, Eq. 7 provides the structure of the $\mathbf{H}_i$ matrix, and guidelines for effects of changing the sensor time resolution and position on the measurement operator $\mathbf{Q}$. Naturally, better time resolution will reduce the mutual coherence. An alternative to improved time resolution which might be technically challenging is to add more sensors as we discuss next.

IV. Optimized Time-Resolved Sensor Array

Using multiple sensors is a natural extension to the single pixel camera. In the case where the sensors are time sensitive, their positioning affects the measurement operator $\mathbf{Q}$ and so it can be optimized. Here we derive an algorithm for sensors placement in an array in order to reduce the mutual coherence of $\mathbf{Q}$. To make the array physically feasible we constrain the sensors to be placed on a single plane $z = 0$. The algorithm accepts two parameters: the number of sensors K and the allowed physical area $\mathcal{C}$, and provides the ideal positions under these constraints.

Starting with Eq. 7, the goal is to maximize the difference between $m(x_1, y_1, t)$ and $m(x_2, y_2, t)$. This is achieved by choosing $r_1 = (x_1, y_1)$, $r_2(x_2, y_2)$ which are furthest apart (this will result in minimal overlap of the rings as shown in Fig. 5).

More precisely, the goal is to select $i = 1..K$ positions r_i within an area $\mathcal{C}$ such that the distance between the sensors is maximized. This can be achieved by maximizing the following objective function:

$$\{r_i\}_{i=1..K} = \underset{\{r_i \in C\}_{i=1..K}}{arg\max} \left\{ \sum_{a=1}^{K} \min_{b \neq a} \|r_a - r_b\| \right\} \qquad (10)$$

Solving Eq. 10 is not tractable. One way to relax this problem is to follow the equivalent of a Max-Lloyd quantizer [27]. This is achieved by following these steps:

1) Initialize K random positions in the allowed area $\mathcal{C}$
2) Repeat until convergence:
   - Calculate the Voronoi diagram of the point set.
   - Move each sensor position to the center of its cell.

To assess the effect of sensor time resolution, number of sensors, and array size on the matrix $\mathbf{Q}$, we evaluate the positioning algorithm for various values of K and sensor area (we assume $\mathcal{C}$ is a square of varying areas). We then build the corresponding $\mathbf{Q}$ matrix and change the sensors' time resolution T. Finally we evaluate the coherence cost objective (Eq. 3). Fig. 6 shows these results. Several key features of the system appear in this analysis: 1) Improving time resolution reduces the number of required sensors non-linearly. 2) It is always beneficial to improve the sensors' time resolution (in this particular example $T < 20ps$ is extremely beneficial — by observing the corresponding curves in Fig. 3 we note that $20ps$ is around the inflection point for the distance $D = 1000cm$). 3) The sensor area defines a maximum number of useful sensors, beyond which there is no significant decrease in the mutual coherence (increasing the array size allows linearly reducing the mutual coherence for a fixed number of sensors). Lastly, by traveling on the isobars it is possible to easily trade-off between different aspects of the system's hardware. For example, a decrease in the sensors' time resolution can be balanced by adding more sensors. This can be useful for realizing an imaging system, seeing as sensors with lower time resolution are cheaper and easier to manufacture. The next section provides another alternative to improving hardware by adding structured illumination.

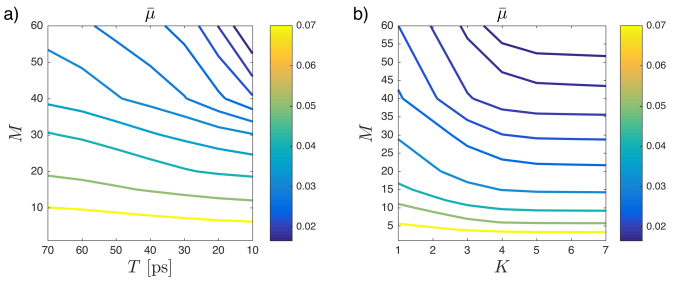

Fig. 7. Effect of number of illumination patterns M, sensor time resolution T and number of sensors K on the mutual coherence $\bar{\mu}$ evaluated with Eq. 3. a) Mutual coherence isobars for a varying number of illumination patterns and sensors' time resolution (for a fixed number of sensors $K = 1$). b) Similar to (a) with a varying number of sensors (for fixed time resolution $T = 20ps$). Both plots are with $\mathcal{C}$ as a square of size $10cm^2$.

V. Optimized Active Illumination for Time-Resolved Sensor Array

We now make the leap to compressive sensing. Previous sections discussed single sensor considerations and sensor placement in an array. This section covers ideal active illumination patterns. We assume the illumination wavefront is amplitude-modulated; this can be physically achieved by an SLM or liquid crystal display (LCD).

When considering different illumination patterns we can choose Hadamard patterns, or as we suggest here — patterns that directly aim to minimize the coherence of the measurement operator. We note that while the mathematical patterns may have negative values, we can only project positive values. In order to achieve the negative values, we can take a measurement with an "all on" pattern and subtract it from the other measurements (due to the linearity of the system) [10].

In order to optimize the illumination pattern, we follow the proposal in [26] and learn the sensing matrix (illumination patterns) in order to directly minimize the coherence of the measurement operator. For example, this concept has been reduced to practice in [28].

The crux of the idea is that given a number of allowed illumination patterns M, we choose the set of illumination patterns that minimizes the mutual coherence of the matrix $\mathbf{Q}$. Since the illumination operator $\mathbf{G}_j$ is only modulating each pixel in the target, it is a diagonal matrix with the pattern values on the diagonal $\mathbf{G}_j = diag\{\mathbf{g}_j\}$, where $\mathbf{g}_j$ is a vector containing the j-th pattern values. Taking a closer look at Eq. 1, we stack all the sensor operators $\mathbf{H}_i$ into $\overline{\mathbf{H}}$ such that:

$$\mathbf{Q} = \begin{bmatrix} \vdots \\ \mathbf{H}_i\mathbf{G}_j \\ \vdots \end{bmatrix} = \begin{bmatrix} \overline{\mathbf{H}}\mathbf{G}_1 \\ \vdots \\ \overline{\mathbf{H}}\mathbf{G}_M \end{bmatrix} = \begin{bmatrix} \overline{\mathbf{H}} \times diag\{\mathbf{g}_1\} \\ \vdots \\ \overline{\mathbf{H}} \times diag\{\mathbf{g}_M\} \end{bmatrix} \qquad (11)$$

Based on Eq. 3, the ideal patterns are the solution to:

$$\{g_j\}_{j=1..M} = \underset{\left\{g_j \in [-1,1]^{L^2}\right\}_{j=1..M}}{arg\min} \left\{ \left\| I_{L^2} - \tilde{Q}^T \tilde{Q} \right\|_F^2 \right\} \qquad (12)$$

This can be solved with standard constrained optimization solvers. Appendix B provides derivation for the cost function and its gradient.

Fig. 7 shows results of experiments for varying the number of allowed illumination patterns, sensors' time resolution, number of sensors, and the effect on the mutual coherence. As predicted by CS theory, increasing the number of patterns has a very strong effect on the mutual coherence. This strong effect allows one to easily relax the demands on hardware requirements when needed. However, as more patterns are allowed, there are increasingly more dependencies on the sensors' parameters. This demonstrates the synergy between compressive sensing and time-resolved sensing. In this case traveling on mutual coherence isobars allows one to trade-off system complexity (cost, size, power) with acquisition time (increased when more patterns are allowed).

Here we only analyzed wavefront amplitude modulation. There are many other ways to use coded active illumination in order to minimize the measurement coherence. For example, we assumed the wavefront is just a pulse in time, but we can perform coding in time domain as well. This will cause different pixels on the target image to be illuminated at different times. Physical implementation of such delays are possible with, for example, fiber bundles (notice that while phase SLM induce varying time delays on the wavefront, these time scales are shorter than current time-resolved sensors resolution). Analysis of such implementation requires detailed care with the interplay between the $\mathbf{H}$ and $\mathbf{G}$ operators (since $\mathbf{G}$ becomes time-dependent), and we leave this analysis to a future study.

VI. Numerical Result

In this section we provide numerical results that show reconstruction using the above analysis. Fig. 8 shows the reconstruction results. We compare our results to the non-time aware single pixel camera (this is equivalent to an $\mathbf{H}$ matrix with just one row with ones), and use of Hadamard illumination patterns. We provide results for several cases of various time resolution and number of sensors. All the results with compressive ultrafast imaging are with the fixed number of illumination patterns — $M = 60$ (i.e. all have the same acquisition time). The scene demonstrated here is sparse in gradient domain. To invert Eq. 1 we use TVAL3 [29]. The reconstruction quality is evaluated with both Peak Signal to Noise ration (PSNR — higher is better, performs pointwise comparison) and Structural Similarity index (SSIM — ranges in $[0, 1]$, higher is better, takes into account the spatial structure of the image [30]).

In order to compare our results to the regular single pixel camera we perform two reconstructions: the first is with the same number of patterns ($M = 60$), which results in the same acquisition time but the scene information is lost. The second is with $M = 2000$, which results in comparable reconstruction quality, but requires $33\times$ longer acquisition time.

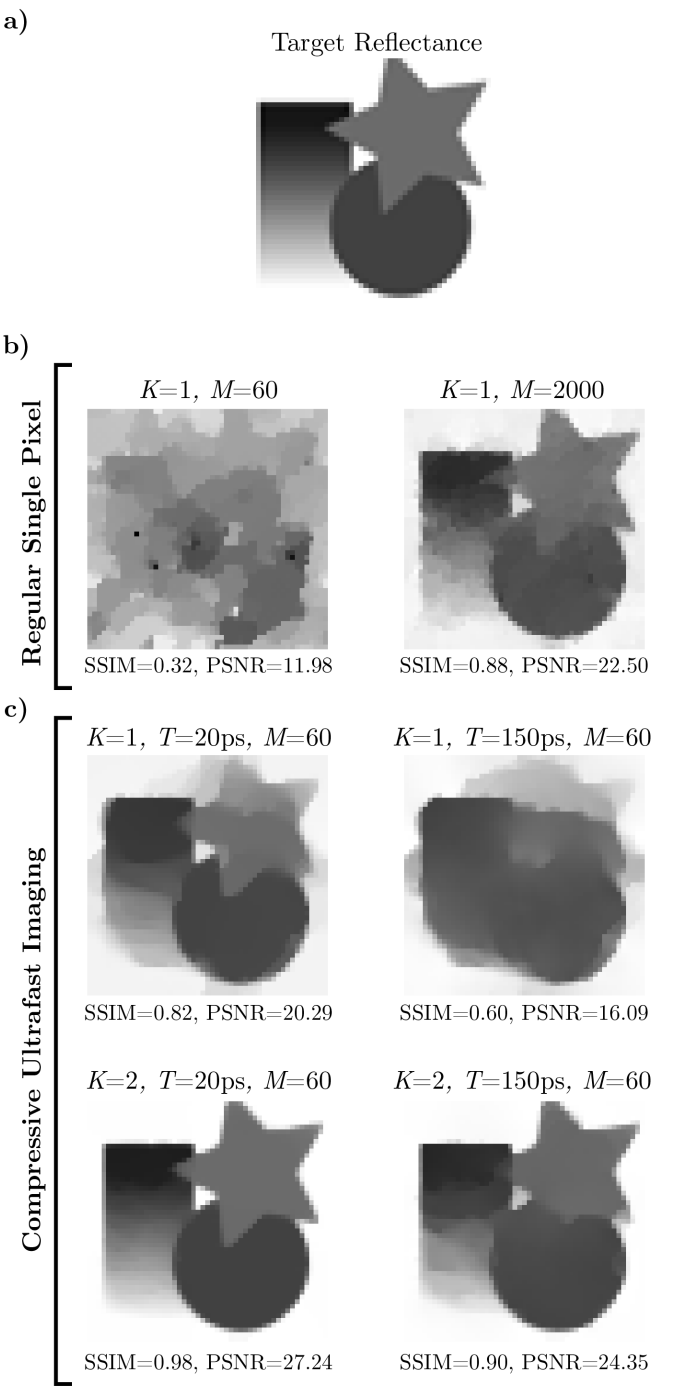

Fig. 8. Imaging with compressive ultrafast sensing. a) The target image (target size is $0.5m^2$ with $10cm$ resolution, located $10m$ from the the sensor plane). b) Result with regular single pixel camera, with $M = 60$ and $M = 2000$. c) Results for single time aware pixel with $T = 20ps$ and $T = 150ps$, shows the strong dependency on time resolution. Result for $K = 2$ pixels with the same time resolutions, shows near perfect reconstruction (based on SSIM).

VII. Conclusion

We demonstrated a novel compressive imaging architecture for using ultrafast sensors with active illumination for lensless imaging. We discussed analysis tools for hardware design, as well as algorithms for ideal sensor placement and illumination patterns which directly target the RIP for robust inversion with compressive deconvolution. The presented approach allows lensless imaging with single pixel and dramatically better acquisition times compared to previous results. This enables novel lensless single pixel imaging in challenging environments. The approach and analysis presented here open new

avenues for other areas with potential tight coupling between novel sensors and compressive sensing algorithms.

APPENDIX A
TIME-RESOLVED SENSORS

Here we provide a short list of time-resolved sensors and their key parameters:

- Time Correlated Single Photon Counter (TCSPC): these devices are usually based on single photon avalanche photodiode (SPAD) which responds to individual photons. Each detected photon is time-tagged with the TCSPC (separate hardware from the SPAD), usually with time resolution on the order of tens of picoseconds. The main advantage of these devices is simplicity and sensitivity.
- Streak camera: steak cameras provide the fastest time resolution — $2ps$. This is achieved by measuring a single line in space, thus providing an $x-t$ image. Unfortunately, streak cameras suffer from poor sensitivity and are relatively costly.
- SPAD array: this is a pixel array of SPAD sensors (on the order of tens of hundreds of pixels) on a single chip. Each pixel includes an embedded TCSPC such that it performs the detection and time tagging. The main advantage is more pixels in the same device, but they suffer from very low fill factor (due to the digital electronics inside the pixel).

APPENDIX B
ILLUMINATION PATTERN OPTIMIZATION ALGORITHM

Here we provide a derivation for calculating the cost function in Eq. 12 and its gradient. Starting with the cost function to minimize:

$$\gamma = \left\| \mathbf{I}_{L^2} - \tilde{\mathbf{Q}}^T \tilde{\mathbf{Q}} \right\|_F^2 \tag{13}$$

Define $\mathbf{\Lambda}$ such that its j-th row is $\mathbf{g}_j$ ($\mathbf{\Lambda}$ is an $M \times L^2$ matrix). Our goal is to find $\mathbf{\Lambda}$ which minimizes γ.

We start by writing: $\mathbf{O} = \tilde{\mathbf{Q}}^T \tilde{\mathbf{Q}}$, and so:

$$\begin{aligned} \gamma &= \|\mathbf{I}_{L^2} - \mathbf{O}\|_F^2 = Tr\left\{ (\mathbf{I}_{L^2} - \mathbf{O}) (\mathbf{I}_{L^2} - \mathbf{O})^T \right\} \\ &= L^2 - 2Tr\{\mathbf{O}\} + Tr\left\{\mathbf{O}\mathbf{O}^T\right\} = \|\mathbf{O}\|_F^2 - L^2 \end{aligned} \tag{14}$$

since $Tr\{\mathbf{O}\} = L^2$. Next, we define $\tilde{\mathbf{Q}} = \mathbf{Q}\mathbf{P}$ where $\mathbf{P}$ is a diagonal matrix with the inverse of the columns norm:

$$\mathbf{P}_{n,n} = \frac{1}{\sqrt{\sum_{a=1}^{MKN} \mathbf{Q}_{a,n}{}^2}} = \frac{1}{\sqrt{\left(\sum_{j=1}^{M} \mathbf{\Lambda}_{j,n}{}^2\right)\left(\sum_{i=1}^{KN} \bar{\mathbf{H}}_{i,n}^2\right)}} \tag{15}$$

This allows us to write:

$$\mathbf{O} = \tilde{\mathbf{Q}}^T \tilde{\mathbf{Q}} = \mathbf{P}^T \mathbf{Q}^T \mathbf{Q} \mathbf{P} = \mathbf{P} \sum_{j=1}^{M} \left(\mathbf{D}_{\mathbf{\Lambda}_j} \bar{\mathbf{H}}^T \bar{\mathbf{H}} \mathbf{D}_{\mathbf{\Lambda}_j}\right) \mathbf{P} \tag{16}$$

where $\mathbf{D}_{\mathbf{\Lambda}_j}$ is a diagonal matrix with the j-th row of $\mathbf{\Lambda}$ on the diagonal. Next we note that:

$$\left[\bar{\mathbf{H}} \mathbf{D}_{\mathbf{\Lambda_j}}\right]_{n,m} = \sum_{a=1}^{L^2} \bar{\mathbf{H}}_{n,a} \left[\mathbf{D}_{\mathbf{\Lambda_j}}\right]_{a,m} = \bar{\mathbf{H}}_{n,m} \mathbf{\Lambda}_{j,m} \tag{17}$$

And:

$$\mathbf{O}_{n,m} = \mathbf{P}_{n,n} \sum_{j=1}^{M} \left(\mathbf{\Lambda}_{j,n} \left[\bar{\mathbf{H}}^{\mathbf{T}} \bar{\mathbf{H}}\right]_{n,m} \mathbf{\Lambda}_{j,m} \right) \mathbf{P}_{m,m} \tag{18}$$

Which can be simplified to:

$$\mathbf{O}_{n,m} = \mathbf{W}_{n,m} \frac{\sum_{j=1}^{M} \mathbf{\Lambda}_{j,n} \mathbf{\Lambda}_{j,m}}{\sqrt{\left(\sum_{j=1}^{M} \mathbf{\Lambda}_{j,n}{}^2\right)\left(\sum_{j=1}^{M} \mathbf{\Lambda}_{j,m}{}^2\right)}} \tag{19}$$

with

$$\mathbf{W}_{n,m} = \frac{\left(\bar{\mathbf{H}}^T \bar{\mathbf{H}}\right)_{n,m}}{\sqrt{\left(\sum_{i=1}^{K} \mathbf{H}_{i,n}{}^2\right)\left(\sum_{i=1}^{K} \mathbf{H}_{i,m}{}^2\right)}} \tag{20}$$

Lastly, we define:

$$\mathbf{\Phi} = \mathbf{\Lambda}^T \mathbf{\Lambda} \tag{21}$$

such that:

$$\mathbf{O}_{n,m} = \mathbf{W}_{n,m} \frac{\mathbf{\Phi}_{n,m}}{\sqrt{\mathbf{\Phi}_{n,n} \mathbf{\Phi}_{m,m}}} \tag{22}$$

Which allows us to write:

$$\mathbf{O} = \left(\sqrt{\mathbf{S}_{\mathbf{\Phi}}}\right)^{-1} (\mathbf{W} \odot \mathbf{\Phi}) \left(\sqrt{\mathbf{S}_{\mathbf{\Phi}}}\right)^{-1} \tag{23}$$

where, $\mathbf{S}_{\mathbf{\Phi}}$ is a diagonal matrix with the diagonal entries of $\mathbf{\Phi}$, and $\odot$ denotes element wise multiplication. Finally:

$$\gamma = \left\| \left(\sqrt{\mathbf{S}_{\mathbf{\Phi}}}\right)^{-1} (\mathbf{W} \odot \mathbf{\Phi}) \left(\sqrt{\mathbf{S}_{\mathbf{\Phi}}}\right)^{-1} \right\|_F^2 - L^2 \tag{24}$$

We note that $\mathbf{W}$ (Eq. 20) is a constant matrix for the illumination pattern optimization and can be calculated a priori. Eq. 21 and 24 provide the final expression for $\gamma(\mathbf{\Lambda})$.

We now develop an expression for the gradient of the cost function. Considering the chain rule for matrices [31]:

$$\left[\frac{d\gamma}{d\mathbf{\Lambda}}\right]_{n,m} = \sum_{a=1}^{L^2} \sum_{b=1}^{L^2} \frac{d\gamma(\mathbf{\Phi})}{d\mathbf{\Phi}_{a,b}} \frac{d\mathbf{\Phi}_{a,b}}{d\mathbf{\Lambda}_{n,m}} \tag{25}$$

Starting with the first term, if $a \neq b$:

$$\frac{d\gamma}{d\mathbf{\Phi}_{a,b}} = \mathbf{W}_{a,b}{}^2 \frac{2\mathbf{\Phi}_{a,b}}{\mathbf{\Phi}_{a,a}\mathbf{\Phi}_{b,b}} \tag{26}$$

and, if $a = b$:

$$\frac{d\gamma}{d\mathbf{\Phi}_{a,a}} = -\sum_{c=1}^{n} \frac{\mathbf{W}_{a,c}{}^2 \mathbf{\Phi}_{a,c}{}^2 + \mathbf{W}_{c,a}{}^2 \mathbf{\Phi}_{c,a}{}^2}{\mathbf{\Phi}_{a,a}{}^2 \mathbf{\Phi}_{c,c}} \delta_{c \neq a} \tag{27}$$

where δ is Kronecker delta. The second term in Eq. 25 is given by [31]:

$$\frac{d\mathbf{\Phi}_{a,b}}{d\mathbf{\Lambda}_{n,m}} = \delta_{mb} \mathbf{\Lambda}_{n,a} + \delta_{ma} \mathbf{\Lambda}_{n,b} \tag{28}$$

Combining Eqs. 25 through 28 we get:

$$\begin{aligned} \left[\frac{d\gamma}{d\mathbf{\Lambda}}\right]_{n,m} &= \sum_{a=1}^{L^2} \sum_{b=1}^{L^2} E^1 \delta_{ab} \left(\delta_{mb} \mathbf{\Lambda}_{n,a} + \delta_{ma} \mathbf{\Lambda}_{n,b}\right) \\ &+ \sum_{a=1}^{L^2} \sum_{b=1}^{L^2} E^2 \delta_{a \neq b} \left(\delta_{mb} \mathbf{\Lambda}_{n,a} + \delta_{ma} \mathbf{\Lambda}_{n,b}\right) \end{aligned} \tag{29}$$

where E^1 and E^2 are the terms in Eqs. 26 and 27 respectively. After some algebra we get:

$$\left[\frac{d\gamma}{d\mathbf{\Lambda}}\right]_{nm} = \frac{2}{\mathbf{\Phi}_{mm}} \sum_{\substack{a=1 \\ a\neq m}}^{L^2} [\frac{\mathbf{\Lambda}_{na}}{\mathbf{\Phi}_{aa}} \left(\mathbf{W}_{am}{}^2 \mathbf{\Phi}_{am} + \mathbf{W}_{ma}{}^2 \mathbf{\Phi}_{ma}\right) - \frac{\mathbf{\Lambda}_{nm}}{\mathbf{\Phi}_{aa}\mathbf{\Phi}_{mm}} \left(\mathbf{W}_{am}{}^2 \mathbf{\Phi}_{am}{}^2 + \mathbf{W}_{ma}{}^2 \mathbf{\Phi}_{ma}{}^2\right)] \quad (30)$$

Lastly, we define:

$$\begin{aligned} \alpha_1 &= \mathbf{W} \odot \mathbf{W} \odot \mathbf{\Phi} \odot \mathbf{I}^- \\ \alpha_2 &= \mathbf{W} \odot \mathbf{W} \odot \mathbf{\Phi} \odot \mathbf{\Phi} \odot \mathbf{I}^- \end{aligned} \quad (31)$$

where, $\mathbf{I}^- = 1 - \mathbf{I}_{L^2}$ (matrix with all ones except for zeros on the diagonal), which allows us to write the final gradient as:

$$\begin{aligned} \mathbf{c}_1 &= \Lambda \mathbf{S}_{\mathbf{\Phi}}{}^{-1} \left(\alpha_1 + \alpha_1{}^T\right) \\ \mathbf{c}_2 &= \left(\mathbf{\Lambda} \odot \left(\mathbf{1}_{M \times L^2} \mathbf{S}_{\mathbf{\Phi}}{}^{-1} \left(\alpha_2 + \alpha_2{}^T\right) \mathbf{S}_{\mathbf{\Phi}}{}^{-1}\right)\right) \\ \frac{d\gamma}{d\mathbf{\Lambda}} &= 2 \left(\mathbf{c}_1 - \mathbf{c}_2\right) \mathbf{S}_{\mathbf{\Phi}}{}^{-1} \end{aligned} \quad (32)$$

where $\mathbf{1}_{M \times L^2}$ is an $M \times L^2$ matrix with all ones.

REFERENCES

[1] D. Donoho, "Compressed sensing," *IEEE Transactions on Information Theory*, vol. 52, no. 4, pp. 1289–1306, apr 2006.

[2] E. J. Candes and T. Tao, "Near-Optimal Signal Recovery From Random Projections: Universal Encoding Strategies?" *IEEE Transactions on Information Theory*, vol. 52, no. 12, pp. 5406–5425, dec 2006.

[3] M. Duarte, M. Davenport, D. Takhar, J. Laska, K. Kelly, and R. Baraniuk, "Single-Pixel Imaging via Compressive Sampling," *IEEE Signal Processing Magazine*, vol. 25, no. 2, pp. 83–91, mar 2008.

[4] I. August, Y. Oiknine, M. AbuLeil, I. Abdulhalim, and A. Stern, "Miniature Compressive Ultra-spectral Imaging System Utilizing a Single Liquid Crystal Phase Retarder," *Scientific Reports*, vol. 6, p. 23524, mar 2016.

[5] A. Szameit, Y. Shechtman, E. Osherovich, E. Bullkich, P. Sidorenko, H. Dana, S. Steiner, E. B. Kley, S. Gazit, T. Cohen-Hyams, S. Shoham, M. Zibulevsky, I. Yavneh, Y. C. Eldar, O. Cohen, and M. Segev, "Sparsity-based single-shot subwavelength coherent diffractive imaging," *Nature Materials*, vol. 11, no. 5, pp. 455–459, apr 2012.

[6] J. Polans, R. P. McNabb, J. A. Izatt, and S. Farsiu, "Compressed wavefront sensing," *Optics Letters*, vol. 39, no. 5, p. 1189, mar 2014.

[7] D. J. Brady, K. Choi, D. L. Marks, R. Horisaki, and S. Lim, "Compressive Holography," *Optics Express*, vol. 17, no. 15, p. 13040, jul 2009.

[8] A. Liutkus, D. Martina, S. Popoff, G. Chardon, O. Katz, G. Lerosey, S. Gigan, L. Daudet, and I. Carron, "Imaging With Nature: Compressive Imaging Using a Multiply Scattering Medium," *Scientific Reports*, vol. 4, p. 489, jul 2014.

[9] C. M. Watts, D. Shrekenhamer, J. Montoya, G. Lipworth, J. Hunt, T. Sleasman, S. Krishna, D. R. Smith, and W. J. Padilla, "Terahertz compressive imaging with metamaterial spatial light modulators," *Nature Photonics*, vol. 8, no. 8, pp. 605–609, jun 2014.

[10] S. Bahmani and J. Romberg, "Compressive Deconvolution in Random Mask Imaging," *IEEE Transactions on Computational Imaging*, vol. 1, no. 4, pp. 236–246, dec 2015.

[11] J. Romberg, "Imaging via Compressive Sampling," *IEEE Signal Processing Magazine*, vol. 25, no. 2, pp. 14–20, mar 2008.

[12] T. B. Pittman, Y. H. Shih, D. V. Strekalov, and A. V. Sergienko, "Optical imaging by means of two-photon quantum entanglement," *Physical Review A*, vol. 52, no. 5, pp. R3429–R3432, nov 1995.

[13] J. Shapiro, "Computational ghost imaging," *Physical Review A*, vol. 78, no. 6, p. 061802, dec 2008.

[14] O. Katz, Y. Bromberg, and Y. Silberberg, "Compressive ghost imaging," *Applied Physics Letters*, vol. 95, no. 13, p. 131110, 2009.

[15] V. Katkovnik and J. Astola, "Compressive sensing computational ghost imaging." *Journal of the Optical Society of America. A, Optics, image science, and vision*, vol. 29, no. 8, pp. 1556–67, aug 2012.

[16] P. Sen, B. Chen, G. Garg, S. R. Marschner, M. Horowitz, M. Levoy, and H. P. A. Lensch, "Dual photography," *ACM Transactions on Graphics*, vol. 24, no. 3, pp. 745–755, jul 2005.

[17] B. Sun, M. P. Edgar, R. Bowman, L. E. Vittert, S. Welsh, a. Bowman, and M. J. Padgett, "3D computational imaging with single-pixel detectors." *Science (New York, N.Y.)*, vol. 340, no. 6134, pp. 844–7, may 2013.

[18] S. S. Welsh, M. P. Edgar, R. Bowman, P. Jonathan, B. Sun, and M. J. Padgett, "Fast full-color computational imaging with single-pixel detectors," *Optics Express*, vol. 21, no. 20, p. 23068, oct 2013.

[19] B. Schwarz, "Lidar: Mapping the world in 3D," *Nature Photonics*, vol. 4, no. 7, pp. 429–430, jul 2010.

[20] A. Kirmani, A. Colaço, F. N. C. Wong, and V. K. Goyal, "Exploiting sparsity in time-of-flight range acquisition using a single time-resolved sensor," *Optics Express*, vol. 19, no. 22, p. 21485, oct 2011.

[21] D. Wu, G. Wetzstein, C. Barsi, T. Willwacher, Q. Dai, and R. Raskar, "Ultra-fast Lensless Computational Imaging through 5D Frequency Analysis of Time-resolved Light Transport," *International Journal of Computer Vision*, vol. 110, no. 2, pp. 128–140, nov 2014.

[22] A. Kirmani, H. Jeelani, V. Montazerhodjat, and V. K. Goyal, "Diffuse imaging: Creating optical images with unfocused time-resolved illumination and sensing," *IEEE Signal Processing Letters*, vol. 19, no. 1, pp. 31–34, jan 2012.

[23] A. Velten, T. Willwacher, O. Gupta, A. Veeraraghavan, M. G. Bawendi, and R. Raskar, "Recovering three-dimensional shape around a corner using ultrafast time-of-flight imaging," *Nature communications*, vol. 3, p. 745, jan 2012.

[24] G. Satat, B. Heshmat, C. Barsi, D. Raviv, O. Chen, M. G. Bawendi, and R. Raskar, "Locating and classifying fluorescent tags behind turbid layers using time-resolved inversion," *Nature Communications*, vol. 6, 2015.

[25] M. Elad, "Optimized projections for compressed sensing," *IEEE Transactions on Signal Processing*, vol. 55, no. 12, pp. 5695–5702, 2007.

[26] J. M. Duarte-Carvajalino and G. Sapiro, "Learning to sense sparse signals: simultaneous sensing matrix and sparsifying dictionary optimization." *IEEE transactions on image processing : a publication of the IEEE Signal Processing Society*, vol. 18, no. 7, pp. 1395–408, jul 2009.

[27] G. Peyré and L. D. Cohen, "Geodesic Remeshing Using Front Propagation," *International Journal of Computer Vision*, vol. 69, no. 1, pp. 145–156, aug 2006.

[28] K. Marwah, G. Wetzstein, Y. Bando, and R. Raskar, "Compressive light field photography using overcomplete dictionaries and optimized projections," *ACM Transactions on Graphics*, vol. 32, no. 4, p. 1, jul 2013.

[29] C. Li, W. Yin, and Y. Zhang, "User's guide for TVAL3: TV minimization by augmented lagrangian and alternating direction algorithms," *CAAM Report*, 2009.

[30] Z. Wang, A. Bovik, H. Sheikh, and E. Simoncelli, "Image Quality Assessment: From Error Visibility to Structural Similarity," *IEEE Transactions on Image Processing*, vol. 13, no. 4, pp. 600–612, apr 2004.

[31] K. B. Petersen, M. S. Pedersen, and Others, "The matrix cookbook," *Technical University of Denmark*, vol. 7, 2008.